Structure and dynamics of the polar vortex in the Earth's core

Binod Sreenivasan
School of Earth and Environment, University of Leeds, Leeds, UK

Chris A. Jones
Department of Applied Mathematics, University of Leeds, Leeds, UK

Received 17 June 2005; revised 8 September 2005; accepted 16 September 2005; published 18 October 2005.

[1] Observations of the Earth's magnetic field suggest that there are anticyclonic polar vortices in the core (Olson and Aurnou, 1999; Hulot et al., 2002). Some geodynamo simulations have also shown the existence of an anticyclonic flow in the polar region of the Earth's outer core. The polar vortices are investigated using a spherical convection-driven dynamo model. In a fully three-dimensional model where no longitudinal symmetry is imposed, we find that the polar vortex core is offset from the pole itself by approximately 10° from the axis of rotation. It is therefore non-axisymmetric, and can drift considerably in longitude during a magnetic diffusion time. We also find that the strong polar vortex depends crucially on the magnetic field in the core. The simulation results are compared with the polar core flow reconstructed from secular variation observations. **Citation:** Sreenivasan, B., and C. A. Jones (2005), Structure and dynamics of the polar vortex in the Earth's core, *Geophys. Res. Lett.*, *32*, L20301, doi:10.1029/2005GL023841.

1. Introduction

[2] The outer core of the Earth is divided into two regions separated by an imaginary cylinder tangent to the inner core boundary and parallel to the Earth's rotation axis. Convection outside the tangent cylinder (TC) is easier to excite, but convection inside the TC can also occur if the temperature gradient between the inner and outer core is large enough. In addition to geodynamo simulations [*Glatzmaier and Roberts*, 1995; *Jones et al.*, 1995; *Olson and Glatzmaier*, 1995; *Olson et al.*, 1999], laboratory experiments on non-magnetic convection between rotating hemispherical shells also show a retrograde (westward) flow near the outer spherical boundary, strongest near the TC [*Aurnou et al.*, 2003]. The secular variation of the geomagnetic field has been used to map the flow beneath the Earth's core-mantle boundary (CMB), using the "frozen flux" approximation [*Roberts and Scott*, 1965]. Studying the secular variation of the radial component of the geomagnetic field over a 120-year period suggested an anticyclonic motion inside the Earth's tangent cylinder with an angular speed of about 0.25° yr^{-1} on average [*Olson and Aurnou*, 1999]. More recently, Oersted and Magsat satellite data were used to interpret variations in the geomagnetic field over twenty years [*Hulot et al.*, 2002]. In the polar regions, generally westward flow of order 0.9° yr^{-1} was found, with the northern hemisphere vortex slightly stronger than the southern hemisphere vortex. It should be noted that the measured flows deduced from the secular variation depend on the assumption of tangential geostrophy and are therefore somewhat uncertain.

[3] This polar azimuthal flow u_ϕ is commonly explained using the thermal wind relation [*Jones*, 2000; *Aurnou et al.*, 2003]

$$2\Omega \frac{\partial u_\phi}{\partial z} = \frac{g\alpha}{r} \frac{\partial T'}{\partial \theta} \tag{1}$$

valid in the regime where inertial effects and Lorentz forces are small compared to the buoyancy and Coriolis forces. In the above equation, Ω is the angular velocity of rotation, g is the acceleration due to gravity and α is the thermal expansion coefficient, θ is the colatitude in spherical polar coordinates, and z is the coordinate parallel to the rotation axis. T' is the temperature fluctuation, that is the departure from the adiabatic value. If the polar regions are on average warmer (less dense) than the regions outside the tangent cylinder, polar fluid near the CMB will rotate westward relative to the polar fluid near the inner core boundary (ICB). If the inner core is gravitationally locked to the mantle [*Buffett and Glatzmaier*, 2000], the assumption we make here, we expect a westward secular variation from the flow just below the CMB. Geodynamo models are generally warmer inside the TC than outside, because outside the TC the thermal boundary layer near the CMB has a much greater surface area than the boundary layer near the ICB, so the mean temperature is near that of the CMB. Inside the TC the mean temperature is closer to the average of the CMB and ICB. Compositional convection can also lower the density inside the TC [*Aurnou et al.*, 2003] as plumes rising off the ICB have on average lower density. However, this thermal wind mechanism ignores magnetic field. While we find that thermal winds can be generated in nonmagnetic simulations, much stronger polar vortices are created through the action of the magnetic field.

2. The Model

[4] In the present model, we consider an electrically conducting fluid between two concentric, co-rotating spherical surfaces that correspond to the ICB and the CMB. The radius ratio is chosen to be 0.35. The super-adiabatic temperatures of the ICB and CMB are maintained at a constant difference ΔT, driving buoyant convection.

0094-8276/05/2005GL023841$05.00

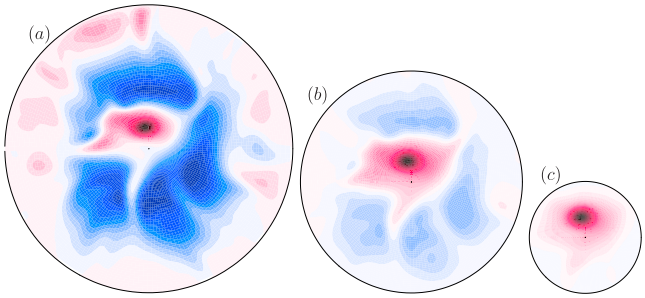

Figure 1. Plots of the temperature perturbation, T' at three horizontal sections above the equatorial plane, $z = 0.9$, 1.2 and 1.46 (shown from left to right). The respective outer radii in dimensionless units are 1.248, 0.962 and 0.485. The tangent cylinder radius is 0.538. No longitudinal symmetry is imposed in this calculation. The red contours represent positive values and blue ones represent negative values. The formation of a localized upwelling centred away from the polar axis can be seen. The minimum and maximum values in the three sections are [−0.131, 0.198], [−0.04, 0.219] and [−0.003, 0.116] respectively.

With the Boussinesq approximation, the time-dependent MHD equations for the velocity $\mathbf{u}$, the magnetic field $\mathbf{B}$ and the temperature T are

$$EPm^{-1}\left(\frac{\partial \mathbf{u}}{\partial t} + (\mathbf{u}\cdot\nabla)\mathbf{u}\right) + 2\mathbf{e}_z \times \mathbf{u} = -\nabla p + Ra\frac{\mathbf{r}}{r_o}T + (\nabla\times\mathbf{B})\times\mathbf{B} + E\nabla^2\mathbf{u}, \quad (2)$$

$$\frac{\partial \mathbf{B}}{\partial t} = \nabla\times(\mathbf{u}\times\mathbf{B}) + \nabla^2\mathbf{B}, \quad (3)$$

$$\frac{\partial T}{\partial t} + (\mathbf{u}\cdot\nabla)T = Pm\, Pr^{-1}\nabla^2 T, \quad (4)$$

$$\nabla\cdot\mathbf{u} = \nabla\cdot\mathbf{B} = 0. \quad (5)$$

The dimensionless groups in the above equations are the Ekman number, $E = \nu/\Omega D^2$, the Prandtl number $Pr = \nu/\kappa$, the modified Rayleigh number $Ra = g\alpha\Delta T D/\eta\Omega$ and the magnetic Prandtl number, $Pm = \nu/\eta$. The gap-width between the shells is D, ν is the kinematic viscosity, κ is the thermal diffusivity, and η is the magnetic diffusivity. The unit of length is D, of time is D^2/η and of temperature is ΔT. Magnetic field is measured in units of $(\rho\Omega\mu\eta)^{1/2}$, ρ being the density and μ the permeability of free space. Several dynamo simulations were performed at a Rayleigh number approximately ten times the critical value needed for the onset of nonmagnetic convection in the spherical shell and the Prandtl numbers Pr and Pm were varied together in the range 0.2–5 in order to study the effect of inertia on the evolution of the vortex. In the results reported here, no longitudinal symmetry is assumed i.e. all azimuthal modes up to the truncation limit ($m = 56$) are included in the calculations. No-slip boundary conditions are imposed at the ICB and CMB, and both inner core and mantle are assumed to be electrically insulating. The code gives close agreement with the dynamo benchmark [*Christensen et al.*, 2001] and other dynamo simulations [*Christensen et al.*, 1999].

3. Results

[5] In Figures 1a–1c, contour plots of the temperature fluctuation are shown for the case $E = 10^{-4}$, $Ra = 750$, $Pr = Pm = 5$, at different constant z sections parallel to the equatorial section. We found that cyclonic polar vortices are generated when the inertial Reynolds stresses are significant. A strong anticyclonic vortex can be realized only for $Pr = Pm \geq 1$, showing that this is a low-inertia phenomenon. A localized hot spot is formed, extending from a region near the inner core boundary right up to the polar region, but offset from the rotation axis. The centre of the hot spot lies on a line closely parallel to the rotation axis. While codes using only even parity azimuthal m-modes are adequate for convection outside the TC [*Christensen et al.*, 1999], they force the polar vortex to lie exactly over the pole and the naturally occurring offset found here is missed.

[6] Upwelling fluid is channelled through the hot spot (see Figure 2a), and is strongly correlated with negative z-vorticity (see Figure 2d). Although smaller hot spots occasionally occur, the flow within the TC is generally dominated by one substantial upwelling plume, and this feature is the main source of the anticyclonic polar vortex in our simulations. This plume changes its longitudinal position with time (see Figures 2b and 2c). The preferred direction of drift is westward, though no fixed velocity of motion can be identified. A region of upwelling can remain locked at an azimuthal position for a long time before moving away to another position. Figure 2e shows the

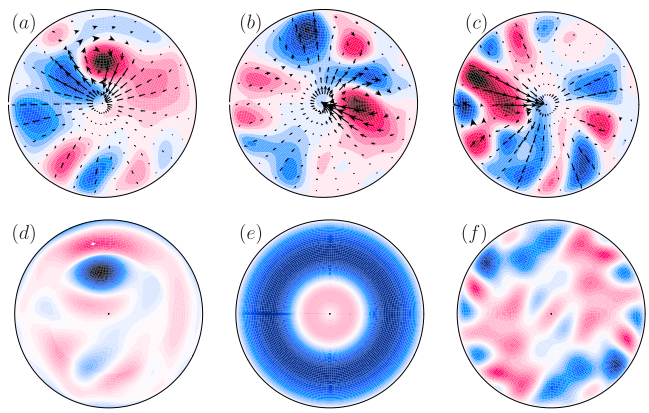

Figure 2. The horizontal section $z = 1.48$ above the equatorial plane. The colour code is as in Figure 1. (a), (b) and (c) are snapshots of u_z with the horizontal velocity arrows superposed at three different times. The times are (a) t_0, the same time as for Figure 1, (b) $t_0 + 0.2\,\tau_d$ and (c) $t_0 + 0.35\tau_d$, where τ_d is the magnetic diffusion time. The respective minimum and maximum values shown are [−21.37, 37.84], [−28.38, 31.24] and [−20.93, 27.64] for u_z. (d) is the z-vorticity at time t_0, with maximum and minimum values [7646, −3059]. (e) is the axisymmetric component of u_ϕ, with maximum and minimum values [−72.3, 20.4]. (f) is the vertical velocity with the magnetic field switched off, but the same parameter values. The maximum and minimum values are only [−3.04, 1.78].

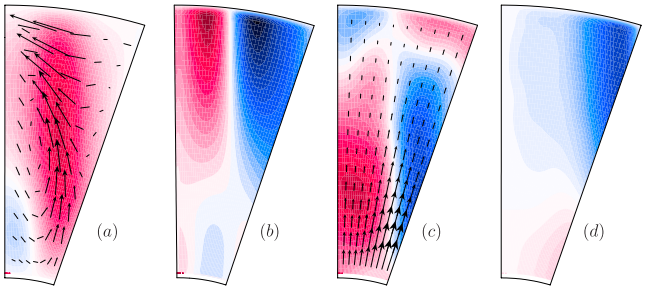

Figure 3. Meridional contour plots in the sector that passes through the centre of the upwelling plume. The sector shown has an angle 18°. The snapshot corresponds to the time t_0 in Figure 2. (a) contours of T', with arrows depicting the meridional velocity. Minimum and maximum temperature [−0.038, 0.205], and maximum meridional velocity (longest arrow) 92.2. (b) azimuthal velocity u_ϕ, with minimum and maximum [−244.1, 206.2]. (c) the azimuthal field B_ϕ, minimum and maximum [−1.262, 1.366], with meridional field arrows superposed. The maximum B_z is 3.462. (d) azimuthal velocity for the nonmagnetic case with the same parameters, minimum and maximum [−20.11, 3.57].

azimuthal average of u_ϕ. The red centre is due to the offset of the vortex producing eastward azimuthal flow between the vortex centre and the axis (see Figure 3b below). However, in the outer part of the polar region the axisymmetric component of flow is dominated by the strong vortex patch leading to anticyclonic circulation.

[7] The off-axis plume creating the anticyclonic vorticity is clearly a convective phenomenon, but it is important to know the relative importance of magnetic and viscous effects in our simulations. In the core, $E \approx 10^{-9}$ is suggested by turbulent viscosity estimates, but numerical stability and resolution requirements impose a much larger E. In the core, the flow must be controlled more by the magnetic field than viscosity, but is this true in our dynamo simulations with $E = 10^{-4}$? To test this, we ran the code with the same parameters but with the magnetic field set to zero. In Figure 2f we show the vertical velocity, which has a large number of plumes all thinner than our magnetic polar vortex plume. The vertical velocity is about ten times weaker. Also, the azimuthal flow for the nonmagnetic case is much weaker than that in the dynamo simulation (compare Figures 3b and 3d). We conclude that magnetic field is very important for the formation of a strong polar vortex. A run was performed with a conducting inner core, the inner core electrical conductivity being equal to the outer core conductivity. We found that the conducting inner core gave a slightly enhanced vortex, but the difference with the insulating inner core case was not very significant.

[8] Figure 3a shows a meridional plot of the temperature perturbation T' with the velocity arrows in the meridional plane. The meridional plot shows the tangent cylinder region magnified in a sector that makes an angle 18° to the vertical axis. The longitude angle of the meridional plane shown is chosen so it passes through the centre of the hot spot, thus maximising the temperature fluctuation and velocity. We see that the offset of the hot spot is about 10°, so that at the CMB it occurs at latitude 80°. The diameter of the vortex core is about 15°. Because of the offset, the azimuthal flow, u_ϕ is prograde (red) between the plume centre and the rotation axis (Figure 3b), but elsewhere the azimuthal flow is retrograde and the net circulation around the TC is negative as shown in Figure 2e. Figure 3c shows contours of the magnetic field B_ϕ and arrows depicting the components of **B** in the meridional plane. B_ϕ appears to be mainly created by u_ϕ twisting the z field component. B_z itself appears to have come mainly from the dipole field generated outside the TC diffusing in. The maximum dimensionless azimuthally averaged $|u_\phi| \approx 70$, observed in our model at a dimensionless distance ≈0.3–0.4 from the rotation axis, could be scaled up to its value in the Earth's core as follows:

$$u_{\phi,\mathrm{sc}} = \frac{u_\phi \eta}{D} = 0.64 \times 10^{-4}\mathrm{ms}^{-1} \approx 0.20^\circ \mathrm{yr}^{-1}, \qquad (6)$$

where η and D have the values 2 m^2 s^{-1} and 2.26×10^6 m. The computed values are slightly lower than the values proposed with the help of secular variation data, but the local u_ϕ can be three times this azimuthally averaged value. Unlike what one sees in models with a freely rotating inner core, there is no significant prograde (eastward) flow near the ICB, though the retrograde flow weakens considerably.

4. Discussion

[9] The linear theory of convection in a horizontal plane layer with the rotation vertical and an imposed vertical magnetic field B_z [*Chandrasekhar*, 1961] provides some insight. In the absence of magnetic field, convection occurs in tall thin columns, somewhat thinner than the polar vortex structure (compare Figures 2a and 2f). In linear theory, the column thickness is related to the horizontal wavenumber a that minimises the critical Rayleigh number, and a depends on the Elsasser number $\Lambda = B_z^2/\mu\rho\Omega\eta$. At small E, as Λ gradually increases, the critical horizontal wavenumber jumps from a large $a \sim 2^{1/6}\pi^{1/3}\ E^{-1/3}/D$ viscous value down to $a \sim \pi/D$ at $\Lambda = \Lambda_c \approx 7.2\ E^{1/3}$. This $O(1)$ value of a is associated with the magnetic mode of convection and corresponds to a larger vortex core than in Figure 2d. As Λ is increased above Λ_c the wavenumber a increases [*Chandrasekhar*, 1961], so we expect the plume to get thinner. Our typical value of Λ is well above Λ_c (see Figure 3c), so our plume is thinner than the radius of the tangent cylinder. Increasing *Ra* increases the generated field strength, and our simulations show that the plume width then decreases. However, dynamo models in our parameter range tend to overestimate the field strength compared to that observed at the CMB, so our plume may be somewhat thinner than that in the Earth's TC.

[10] To understand why the magnetic field influences the vortex so strongly, we consider the dynamics of an axisymmetric plume. The angular momentum equation is

$$2\Omega u_s = \frac{1}{\mu\rho s}\mathbf{B}\cdot\nabla\left(sB_\phi\right) + \nu\left(\nabla^2 u_\phi - \frac{u_\phi}{s^2}\right), \qquad (7)$$

where s is the radius in cylinder polar coordinates. The convergent and divergent horizontal parts of the flow in the plume near the ICB and CMB respectively advect planetary vorticity, producing cyclonic vorticity near the ICB and anticyclonic vorticity near the CMB. With no magnetic field

this process is balanced only by viscosity, resulting in many very thin plumes. The magnetic field can balance planetary vorticity advection without the need for small horizontal length-scales. The thermal wind equation (1) acquires an additional magnetic wind term,

$$2\rho\Omega\frac{\partial u_\phi}{\partial z} = \frac{\rho g\alpha}{r}\frac{\partial T'}{\partial \theta} - \mathbf{e}_\phi \cdot \nabla \times (\mathbf{j} \times \mathbf{B}). \quad (8)$$

The more powerful vortex in the magnetic case is driven mainly by an enhanced thermal wind, the magnetic wind being only of the same order as the thermal wind.

[11] The strength of our simulated vortex is on the low side compared with the observations, as the estimate (6) gives 0.20° yr^{-1}, while the secular variation observations suggested typical values of 0.25° yr^{-1} and 0.9° yr^{-1}. However, estimates of the heat flux through the core (which itself is not very precisely constrained) suggest that *Ra* should be $O(10^4)$, roughly ten times our value. Such a large value of *Ra* is not feasible with currently available computer technology. We would expect that a larger *Ra* will enhance the strength of the convective plume, which might lead to a somewhat stronger vortex than our *Ra* = 750 calculations predict. Simulations with more geophysically relevant parameters might produce a better agreement for the vortex angular velocity. An off-centre vortex patch of a similar size to that produced in our simulations is visible inside the TC in the northern hemisphere (but not in the southern hemisphere) in the Oersted-Magsat secular variation data [*Hulot et al.*, 2002] at longitude 45° east.

[12] **Acknowledgments.** This work was sponsored by a grant from the UK Particle Physics and Astronomy Research Council. The computational work was performed on the MHD clusters at Universities of Exeter and St. Andrews.

References

Aurnou, J., S. Andreadis, L. Zhu, and P. Olson (2003), Experiments on convection in the Earth's core tangent cylinder, *Earth Planet. Sci. Lett.*, *212*, 119–134.

Buffett, B. A., and G. A. Glatzmaier (2000), Gravitational braking of inner-core rotation in geodynamo simulations, *Geophys. Res. Lett.*, *27*, 3125–3128.

Chandrasekhar, S. (1961), *Hydrodynamic and Hydromagnetic Stability*, Clarendon, Oxford, U. K.

Christensen, U., P. Olson, and G. A. Glatzmaier (1999), Numerical modelling of the geodynamo: A systematic parameter study, *Geophys. J. Int.*, *138*, 393–409.

Christensen, U. R., et al. (2001), A numerical dynamo benchmark, *Phys. Earth Planet. Inter.*, *128*, 25–34.

Glatzmaier, G. A., and P. H. Roberts (1995), A three-dimensional convective dynamo solution with rotating and finitely conducting inner core and mantle, *Phys. Earth Planet. Inter.*, *91*, 63–75.

Hulot, G., C. Eymin, B. Langlais, M. Mandea, and N. Olsen (2002), Small-scale structure of the geodynamo inferred from Oersted and Magsat satellite data, *Nature*, *416*, 620–623.

Jones, C. A. (2000), Convection driven geodynamo models, *Philos. Trans. R. Soc. London*, *358*, 873–897.

Jones, C. A., A. W. Longbottom, and R. Hollerbach (1995), A self-consistent convection driven geodynamo model, using a mean field approximation, *Phys. Earth Planet. Inter.*, *92*, 119–141.

Olson, P., and J. Aurnou (1999), A polar vortex in the Earth's core, *Nature*, *402*, 170–173.

Olson, P., and G. A. Glatzmaier (1995), Magnetoconvection in a rotating spherical shell: Structure of flow in the outer core, *Phys. Earth Planet. Inter.*, *92*, 109–118.

Olson, P., U. Christensen, and G. A. Glatzmaier (1999), Numerical modeling of the geodynamo: Mechanisms of field generation and equilibration, *J. Geophys. Res.*, *104*, 10,383–10,404.

Roberts, P. H., and S. Scott (1965), On the analysis of the secular variation. I. A hydromagnetic constraint theory, *J. Geomagn. Geoelectr.*, *17*, 137–151.

C. A. Jones, Department of Applied Mathematics, University of Leeds, Leeds LS2 9JT, UK.

B. Sreenivasan, School of Earth and Environment, University of Leeds, Leeds LS2 9JT, UK. (binod@earth.leeds.ac.uk)